# Geometric system analysis of ILMD-based LID measurement systems using Monte-Carlo simulation



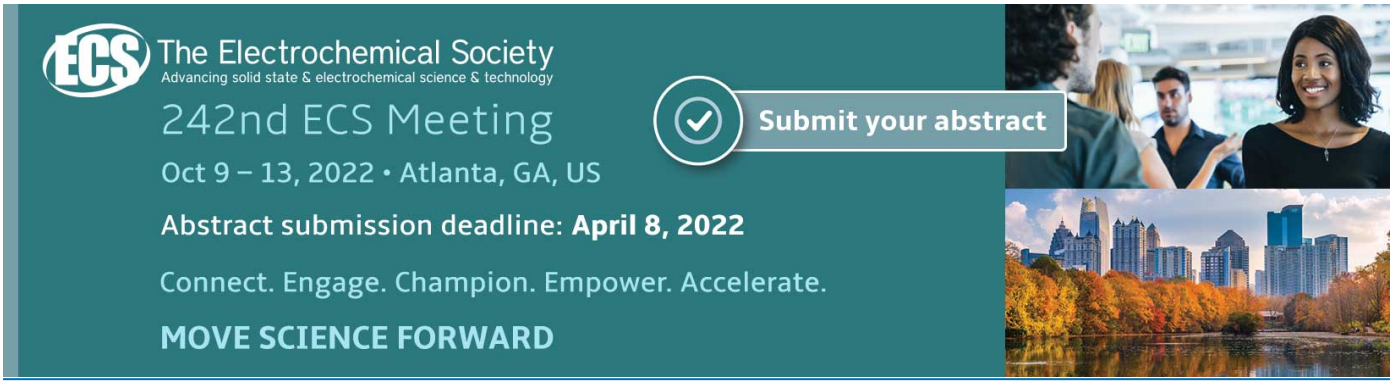

# Geometric system analysis of ILMD-based LID measurement systems using Monte-Carlo simulation

**M Katona[1], K Trampert[1], C Schwanengel[2], U Krüger[2] and C Neumann[1]**

[1]Karlsruhe Institute of Technology (KIT), Karlsruhe, Germany
[2]TechnoTeam Bildverarbeitung GmbH, Ilmenau, Germany

Corresponding e-mail address: markus.katona@kit.edu

**Abstract**. Imaging Luminance Measuring Device (ILMD) based luminous intensity distribution measurement systems are an established method for measuring the luminous intensity distribution (LID) of light sources in the far field. The advantage of this system is the high-resolution acquisition of a large angular range with one image. For the uncertainty budget, the mathematical description of the system can be divided into photometric and geometric contributions. In the following, we will present a Monte-Carlo approach to analyse the geometric contributions which are the uncertainty of measurement direction and measurement distance. Therefore, we set up a geometric system description based on kinematic transformations that describes the connection between detector and light source position. To consider all relevant input quantities we simulate the adjustment and measurement process. Finally, an analysis of the geometric input parameters is shown.

## 1. Introduction

The LID $I(\varphi, \vartheta)$ is the luminous flux $\Phi$ per solid angle $\Omega$ that is emitted in the direction $(\varphi, \vartheta)$ [1].

$$I(\varphi, \vartheta) = \frac{\mathrm{d}\Phi(\varphi, \vartheta)}{\mathrm{d}\Omega(\varphi, \vartheta)}. \quad (1)$$

Hence a solid angle is just defined for a point, the necessary assumption of the light source (device under test (DUT)) is a point source. This indicates that the measurement distance has to be greater than the dimensions of the DUT so that the photometric distance law is satisfied. The photometric distance law is given by:

$$I = \frac{E \cdot r^2}{\cos(\varepsilon)}, \quad (2)$$

where $E$ represents the illuminance on a photometer detector that is proportional to the luminous intensity by considering the measurement distance $r$ to the power of two. The term $\cos(\varepsilon)$ defines the angle of incidence of the detector [1].

Common methods to measure the LID are far-field goniophotometers, e.g. an ILMD measurement system [2–4]. For this method, a DUT is mounted on a goniophotometer and illuminates a lambertian reflecting flat white screen in a large distance (see Figure 1). The screen represents the detector surface and an ILMD measures the luminance on the screen. Knowing the geometric relation between the system components, it is possible to calculate the LID in the angular range of the screen.

If the angular range of interest is larger than the screen, the recorded LID of one single measurement corresponds only to a LID-segment. To obtain the LID of any size the goniometer rotates the DUT in

multiple viewing directions by the horizontal and vertical rotation axis coordinates $(H, V)$. As a result, each desired direction is once seen by the screen (see Figure 2). Afterwards an image-stitching algorithm stiches together the recorded LID-segments [3, 4].

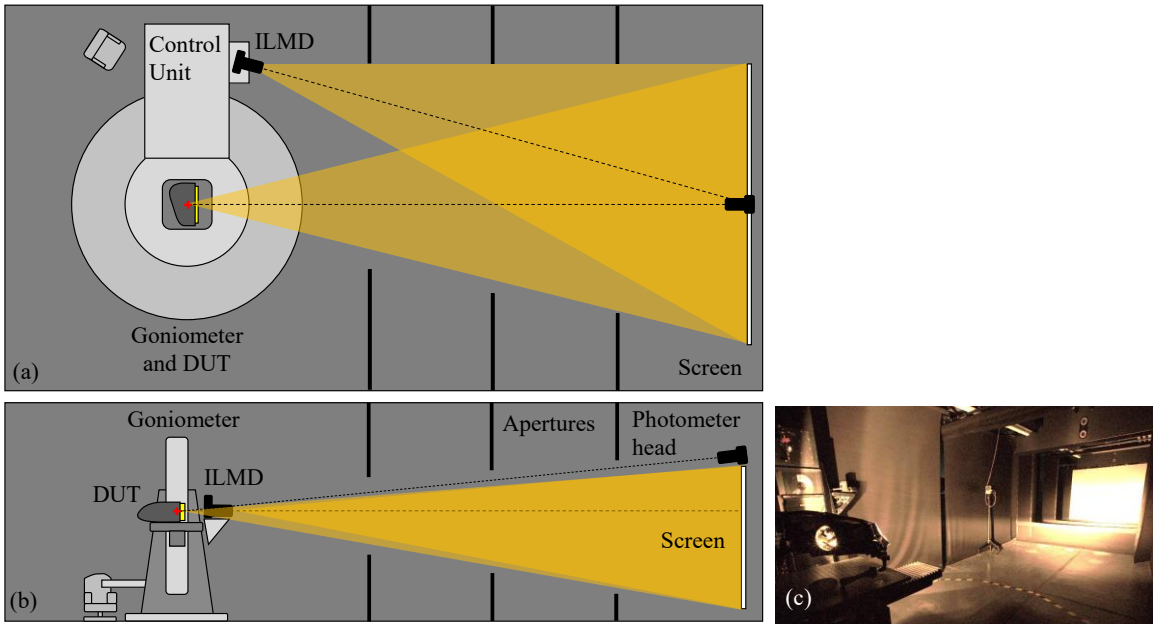


**Figure 1**: ILMD-based LID measurement system at *Light Technology Institute (LTI)* at *KIT*, illustrated as bird view (a) and side view (b). (c) shows an image of the measurement system.

Nevertheless, there are uncertainty contributions to each LID measurement that are caused by photometric as well as geometric system components. Photometric components influence the determined photometric measurand $E$, e.g. stray light. Geometric components involve all components that influences the measurement direction $(\varphi, \vartheta)$ as well as the measurement distance $r$. These components include the spatial position of the detector (e.g. the screen), the spatial position of the goniometer, the intrinsic uncertainties of the goniometer (e.g. the goniometer-axis position accuracy during the measurement) and the position of the DUT as well as the position of the adjustment standards. In the following, we will present a method to determine the geometric uncertainty parameters by guidelines of „*Guide to the Expression of Uncertainty in Measurement*“ (GUM) [5, 6]. This will be done by the Monte-Carlo-Method (MCM) based on an approach of B. Jokiel Jr, et al. for parallel kinematic machines [7]. A similar approach was published already in M. Katona, et al. [8]. However the presented work is much broader and covers more detailed aspects e.g. the adjustment process.

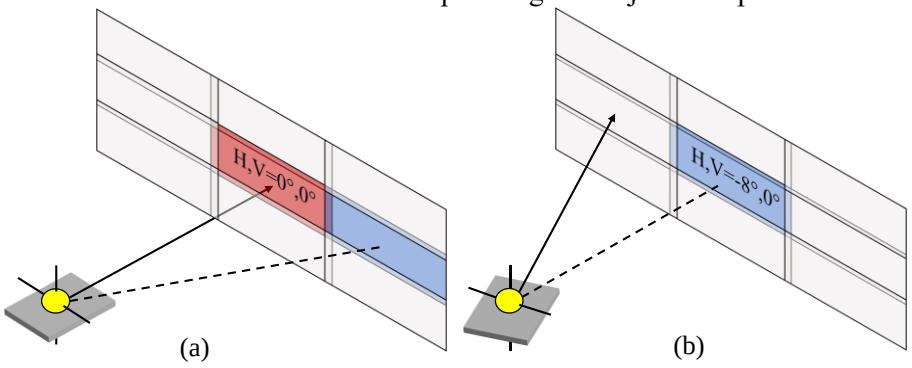


**Figure 2**: Schematic representation of the image stitching algorithm for composing LIDs with a larger angular range than the screen. (a) and (b) are showing two different goniometer recording positions.

## 2. Geometric adjustment

To simulate an overall measurement process, it is necessary to consider the adjustment process of the LID measurement system. In our case, the geometric adjustment assigns angular directions to camera (or screen) pixels. For this we use an angle standard. This is a laser matrix, which is adjusted in the goniometer rotation center and aligned along the optical axis. Knowing the angular position of the laser matrix points it is possible to assign camera pixels to spatial directions unambiguously. Figure 3 illustrates this method. The uncertainty resulting from this method is due to the positioning accuracy of the angle standard on the goniometer and the uncertainty of the angle standard itself.

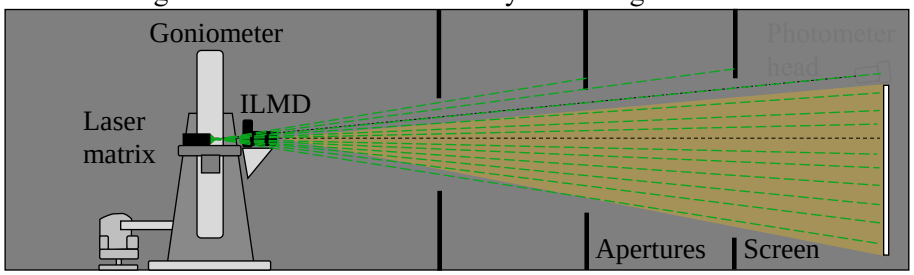


**Figure 3**: Adjustment process of ILMD-based LID measuring system at *LTI*.

## 3. Measurement Model

For an uncertainty analysis of LID measurements according to GUM a measurement model is necessary. For this the basic model is the photometric distance law according to equation (2):

$$I = k_{\mathrm{E}} \cdot Y_{\mathrm{E}}(\varphi, \vartheta) \cdot r^2. \tag{3}$$

Neglecting the detectors orientation and assuming it to be orthogonal to the centre of the goniometer, the LID $I$ is calculated from the detector return value $Y_{\mathrm{E}}$ of the measurement direction $(\varphi, \vartheta)$, the calibration factor $k_{\mathrm{E}}$ and the measurement distance $r$. It should be noted that arbitrarily more detailed models can be set up [9, 10]. Nevertheless, the example of the basic model shows that there are three geometric input quantities $(\varphi, \vartheta, r)$ that have an influence on the measurement result. The uncertainty of the measurement direction $(u(\varphi), u(\vartheta))$ as well as the uncertainty of the measurement distance $u(r)$ contribute to the combined measurement uncertainty of a LID.

To obtain the geometric uncertainty, $(\varphi, \vartheta, r)$ can also be described as the detector position of a measured direction in the coordinate system of the DUT. For spherical coordinates this position is $\boldsymbol{p}_{\mathbf{S\,sph}} = (\varphi, \vartheta, r)$. The index 'S' stands for "source" and 'sph' for "spherical". Expressed in cartesian coordinates this is $\boldsymbol{p}_{\mathbf{S}} = (x, y, z)$ [11, 12], which can be calculated using a kinematic chain of the measurement system that connects the position of the DUT and the detector during a measurement. The convention of the coordinate systems we use in the following are presented in Figure 4.

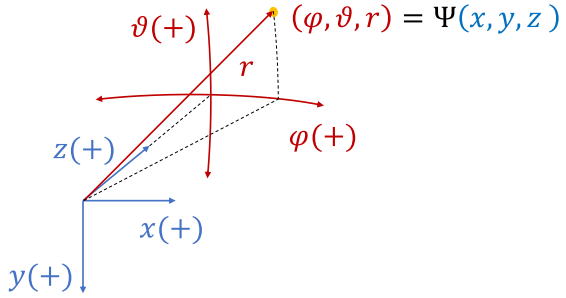


**Figure 4**: Convention of the used coordinate systems.

### *3.1. Kinematic chain*

For this purpose, we set up a kinematic chain to transform a point in the coordinate system of the source e.g. $\boldsymbol{q}_{\mathbf{S}}$ in the coordinate system of the detector $\boldsymbol{q}_{\mathbf{D}}$ including all geometric measurement components. In this case 'D' stands for detector. This transformation is given by

$$\boldsymbol{q}_{\mathbf{D}} = \boldsymbol{T}_{\mathbf{system}} \cdot \boldsymbol{q}_{\mathbf{S}}{}^{\mathrm{T}}. \tag{4}$$

where $\boldsymbol{T}_{\mathbf{system}}$ represents the combined transformation chain that includes all individual transformations of the measurement system

$$\boldsymbol{T}_{\mathbf{system}} = \boldsymbol{T}_{\mathbf{n-1 \to n}} \cdot \ldots \boldsymbol{T}_{\mathbf{i}} \cdot \ldots \cdot \boldsymbol{T}_{\mathbf{1 \to 2}}. \tag{5}$$

Each individual transformation $\boldsymbol{T}_{\mathbf{i}}$, in turn, consisting out of translations $\boldsymbol{t}_{\mathbf{i}}$ and rotations given by the 3x3 rotation matrix $\boldsymbol{R}_{\mathbf{i}}$ [13]:

$$\boldsymbol{T}_{\mathbf{i}} = \begin{pmatrix} \boldsymbol{R}_{\mathbf{i}} & \boldsymbol{t}_{\mathbf{i}} \\ 0_{1x3} & 1 \end{pmatrix} \quad \boldsymbol{R}_{\mathbf{i}} = \begin{pmatrix} r_{11} & r_{12} & r_{13} \\ r_{21} & r_{22} & r_{23} \\ r_{31} & r_{32} & r_{33} \end{pmatrix} \quad \boldsymbol{t}_{\mathbf{i}} = \begin{pmatrix} x \\ y \\ z \end{pmatrix} \tag{6}$$

The necessary components for a casual LID far-field goniophotometer are the detector $X_{\mathrm{D}}$, the goniometer $X_{\mathrm{G}}$ and the source $X_{\mathrm{S}}$. If the goniometer is a conventional two axes rotation stage, the goniometer can be expressed as two components, which are the vertical- and horizontal rotation axes $X_{\mathrm{G\,V}}$ and $X_{\mathrm{G\,H}}$. Table 1 lists all necessary components of a standard conventional measurement.

**Table 1**: System components of a conventional LID far-field measurement system.

| Nr. | Coordinate system | Symbol |
|---|---|---|
| 1 | Source | $X_{\mathrm{S}}$ |
| 2 | Goniometer H-axis | $X_{\mathrm{G\,H}}$ |
| 3 | Goniometer V-axis | $X_{\mathrm{G\,V}}$ |
| 4 | Detector | $X_{\mathrm{D}}$ |

In order to set up the kinematic model of the measurement system under investigation, all measurement components need to be described as exact as possible. This includes all sub-transformations to transform each component in the position of the previous component. In some cases it is possible to use existing data-files, e.g. models that describe the goniometer in robot kinematics. In other cases such data-files are not given or this is less practicable. Then it is necessary to design the components themselves and consider all important degrees of freedom. Hence it may be also advantageous to reduce the model to necessary input quantities. This can be done by following steps:

- Describe the system with all geometric parameters from the detector position to the DUT.
- Determine which sub-transformations are “static” and which are “variable”.
- Note that “static” as well as “variable” input quantities are subject to uncertainty.
- “Static” sub-transformations are not changing over time, this is e.g. the pose between goniometer and detector or the pose between the two goniometer axes.
- ”Variable” sub-transformations are changing in between different measurements or during the measurement process e.g. the DUT position on the goniometer or axes-position.
- If possible, it might be an advantage to summarize “static” sub-transformation.
- To define a sub-transformation as “static” tests must be performed.

Following these rules to set up a kinematic chain of the ILMD based LID measurement system we have to consider the five axes type A goniometer and a flat white screen in about 10 m distance. Figure 5 shows the measurement system as well as the necessary kinematic transformations. Because the three goniometer linear axes are locked during the measurement, it is sufficient to describe the system by four necessary components according to Table 1. Hence, the necessary kinematic chain is:

$$\boldsymbol{T}_{\mathbf{system}} = \boldsymbol{T}_{\mathbf{G\,V\,static}} \cdot \boldsymbol{T}_{\mathbf{G\,V\,var}} \cdot \boldsymbol{T}_{\mathbf{G\,H\,static}} \cdot \boldsymbol{T}_{\mathbf{G\,H\,var}} \cdot \boldsymbol{T}_{\mathbf{S}} \tag{7}$$

Here, the transformation $\boldsymbol{T}_{\mathbf{S}}$ indicates the position of the source with respect to the goniometer H-axis. During a measurement the source is considered to be perfectly aligned in the goniometer rotation centre. In reality, however, the source can be misaligned in each direction $(x_{\mathrm{S}}, y_{\mathrm{S}}, z_{\mathrm{S}})$ as well as misoriented around each coordinate system axis $(\theta_{\mathrm{x\,S}}, \theta_{\mathrm{y\,S}}, \theta_{\mathrm{z\,S}})$. The transformations $\boldsymbol{T}_{\mathbf{G\,H\,var}}$ and $\boldsymbol{T}_{\mathbf{G\,V\,var}}$ specify the rotation positioning of the H- and V-axis, respectively. Hereby the H-axis rotation is a rotation around the y-axis (compare Figure 4 and Figure 5) including the goniometer coordinate *H*

as well as an uncertainty value. The V-axis rotation is a rotation around the x-axis. $\boldsymbol{T}_{\mathbf{G\,H\,static}}$ describes the misalignment between the H- and V-axis, represented sufficiently by two parameters, an axial distance in z-direction and an axial tilt around the z-axis. Finally, the transformation $\boldsymbol{T}_{\mathbf{G\,V\,static}}$ describes the position of the V-axis with respect to the detector. Therefore, all six degrees of freedom are used.

Due to solid components of the goniometer, we do not consider any thermal or mechanical deformation of this goniometer. In fact, it has to be noted, that, if necessary, it is simple to include this parameter as input quantities as well.

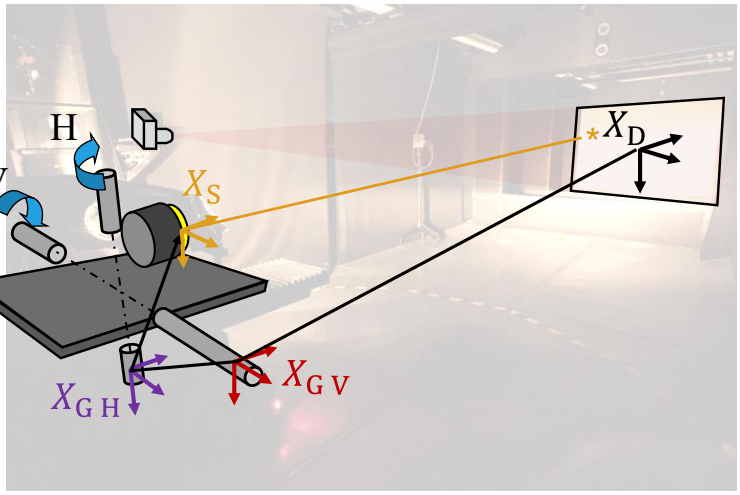


**Figure 5:** ILMD-based LID measuring system at *LTI*.

*3.2. Measurement and adjustment process*

With the described model it is possible to calculate the position and orientation of a DUT in the coordinate system of the detector or the other way around. By assuming the detectors surface as the xy-plane, we can calculate the actual detector position in the coordinate system of the DUT. For this a simple ray-plane intersection is used. Executing this model in the combination with a Mote-Carlo-Simulation the result is a set of detector positions that can be statistically evaluated. Nevertheless, this procedure is already described in [8] but not considering the adjustment process.

In order to represent the entire measurement process beside the measurement it is necessary to simulate the adjustment process as well. In both processes input variables provide a measurement uncertainty contribution. Moreover, correlation between input variables of both processes are considered. E.g. the goniometer-screen distance is the same during both processes, by means an associated uncertainty will not influence the measurement.

Considering also the adjustment, we use the kinematic model twice. In the first step we calculate the real detector position in the coordinate system of the detector by simulating the adjustment process, which is shown in Figure 6. Considering all uncertainties of the kinematic chain we obtain the position of the source (laser matrix) in the coordinate system of the detector. If we now assume the screen to be in the xy-plane and simulate the laser matrix we obtain detector positions $\boldsymbol{p}_{\mathbf{D}}$ by line-plane intersection. The laser matrix is simulated by target directions $(\varphi, \vartheta)_{\mathrm{target\,0}}$ as well as the laser matrix uncertainties. In fact the obtained detector positions include the uncertainty of the laser matrix, this position is not labeled as 'target'. This process is usually done in goniometer rotation position $(H, V) = (0°, 0°)$.

In the second step we simulate the measurement process (see Figure 7), using the kinematic model again. We choose the similar "static" transformations as in the adjustment process. For the "variable" transformations we have to use different uncertainty values. Simulating all goniometer positions $(H, V)$, we obtain the actual detector position $\boldsymbol{p}_{\mathbf{S\,actual}}$ for each measured direction in the coordinate system of the DUT. It should be noted, that the target directions of the DUT $(\varphi, \vartheta)_{\mathrm{target}}$ are calculated using the target direction of the adjustment process $(\varphi, \vartheta)_{\mathrm{target\,0}}$ and the goniometer position coordinates $(H, V)$.

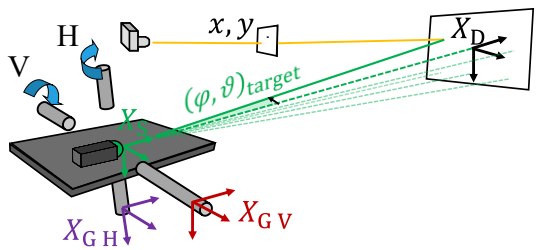


Figure 6: Kinematic model to simulate the adjustment process.

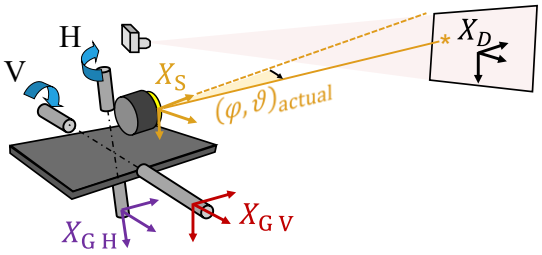


**Figure 7:** Kinematic model to simulate the measurement process.

## 4. Monte-Carlo-Simulation

To calculate the geometric uncertainty from the described model we use the MCM according to GUM Supplement 2 [6]. Therefore, a set of $M = 10000$ actual detector positions $\boldsymbol{p}_{\mathbf{S\,actual\,m}}$ is calculated for each target direction. $M$ corresponds to the number of Monte-Carlo iterations and $m$ is the current simulation step. The used parameters and its uncertainty values are listed in Table 2. As previously described, it is necessary to consider the same input uncertainties for the adjustment and the measurement process, when it comes to static parameters. In our case static parameters are: the distance and tilt between the goniometer H and V-axis (no. 8, 9) and the position and orientation between screen and goniometer V-axis (no. 11-13). Variable parameters are: the DUT position and orientation (no. 1-6), the goniometer axes position during measurement process (no. 7, 10), the laser matrix position and orientation (no. 14-19) and the goniometer axes position during adjustment process (no. 20, 21).

**Table 2:** Geometric uncertainty budget of the measurement system determined by MCM.

| No | Component | Transformation | Trans-formation type | Axis | Unit | Esti-mate | Dist. | Standard un-certainty | Max. absolute contribution of direction | Max. absolute contribution of distance |
|---|---|---|---|---|---|---|---|---|---|---|
| $i$ | | input $X_i$ | | | | $\xi_i$ | $g_{\xi_i}$ | $u(\xi_i)$ | $u(l)$ in [°] | $u(r)$ in [mm] |
| 1 | DUT | orientation | variable | $x$ | ° | 0 | N | 0.25 | 0.25 | 0 |
| 2 | | | | $y$ | ° | 0 | N | 0.25 | 0.25 | 0 |
| 3 | | | | $z$ | ° | 0 | N | 0.25 | 0.24 | 0 |
| 4 | | position | variable | $x$ | mm | 0 | N | 10 | 0.057 | 9.91 |
| 5 | | | | $y$ | mm | 0 | N | 10 | 0.057 | 9.89 |
| 6 | | | | $z$ | mm | 0 | N | 10 | 0.057 | 9.96 |
| 7 | Goniometer H-axis | rotation H | variable | $y$ | ° | H | N | 0.0031 | 0.0031 | 0 |
| 8 | | axis tilt | static | $z$ | ° | 0 | N | 0.008 | 0.0086 | $10^{-6}$ |
| 9 | | axis distance | | $z$ | mm | 0.5 | N | 0.052 | 0.0001 | 0.05 |
| 10 | Goniometer V-axis | rotation V | variable | $x$ | ° | V | N | 0.0041 | 0.0041 | $10^{-5}$ |
| 11 | | Screen distance | static | $z$ | mm | 10000 | N | 2 | $10^{-7}$ | 0 |
| 12 | | orientation | static | $x$ | ° | 0 | N | 0.1 | $10^{-7}$ | 0 |
| 13 | | | | $y$ | ° | 0 | N | 0.1 | $10^{-7}$ | 0 |
| 14 | Laser matrix adjustment | orientation | variable | $x$ | ° | 0 | N | 0.25 | 0.25 | $10^{-3}$ |
| 15 | | | | $y$ | ° | 0 | N | 0.25 | 0.25 | $10^{-4}$ |
| 16 | | | | $z$ | ° | 0 | N | 0.25 | 0.038 | $10^{-4}$ |
| 17 | | position | variable | $x$ | mm | 0 | N | 1 | 0.0058 | 0.14 |
| 18 | | | | $y$ | mm | 0 | N | 1 | 0.0058 | 0.09 |
| 19 | | | | $z$ | mm | 0 | N | 1 | 0.0009 | 0.99 |
| 20 | Goniometer H-axis adjustment | rotation H | variable | $y$ | ° | 0 | N | 0.0031 | 0.0031 | $10^{-6}$ |
| 21 | Goniometer V-axis adjustment | rotation V | variable | $x$ | ° | 0 | N | 0.0041 | 0.0041 | $10^{-5}$ |
| 22 | Laser points adjustment | orientation | variable | $y$ | ° | $\varphi_{\text{target 0}}$ | N | 0.002 | 0.002 | $10^{-6}$ |
| 23 | | | | $x$ | ° | $\vartheta_{\text{target 0}}$ | N | 0.002 | 0.002 | $10^{-6}$ |
| 24 | Total system (k=2.45) | | | | | | | | 0.36<br>0.78 | 10.11<br>24.77 |
| 25 | Total system by obtaining ideal DUT and laser matrix alignment (k=2.45) | | | | | | | | 0.0093<br>0.023 | 0.02<br>0.049 |

It is necessary to mention, that we determined the estimates and uncertainties of the input quantities from Table 2 using some simple methods, which are not described in detail. Beside laser distance meter and lasers we used pattern recognition in image processing algorithms. The parameters concerning the DUT and laser matrix pose are based on empirical values. Especially the DUT positioning uncertainty of 10 mm is quite a high value. However, this is based on the determination of the photometric center, which may be difficult to determine in some cases.

After the Monte-Carlo process the obtained set of detector positions has to be evaluated statistically. For this it is necessary to rotate each set of detector positions $\boldsymbol{p}_{\mathbf{S\ actual\ m}}$ to the optical axis of the DUT using the target positions $(\varphi, \vartheta)_{\mathrm{target}}$. Otherwise a conversion from detector positions to measurement directions may results in a misinterpretation of the angular uncertainty due to angle distortion of spherical coordinates at the poles. As shown in Figure 8 it is possible to convert each set of detector position in a measurement distance uncertainty, which is the standard deviation $\sigma_{\mathrm{r}}$ along the measurement direction. For the measurement direction we use an elliptical confidence region from the covariance matrix of all coordinates $(\varphi, \vartheta)_{\mathrm{actual}}$ [6]. The measurement direction uncertainty is then given by the standard deviation along the large ('$l$') ellipse axis $u(l) = \sigma_{\mathrm{l}}$ and the standard deviation along the short ('$s$') ellipse axis $u(s) = \sigma_{\mathrm{s}}$. To give full correlation information it is also possible to represent the angle $\alpha$ of the confidence ellipse. The use of the uncertainty description along the large and short ellipse axis of the confidence region instead of uncertainties along $\varphi$- and $\vartheta$-coordinate axes is also due to arrangement of the spherical coordinates at the pole. Coordinates at the pole are distorted with respect to the equator.

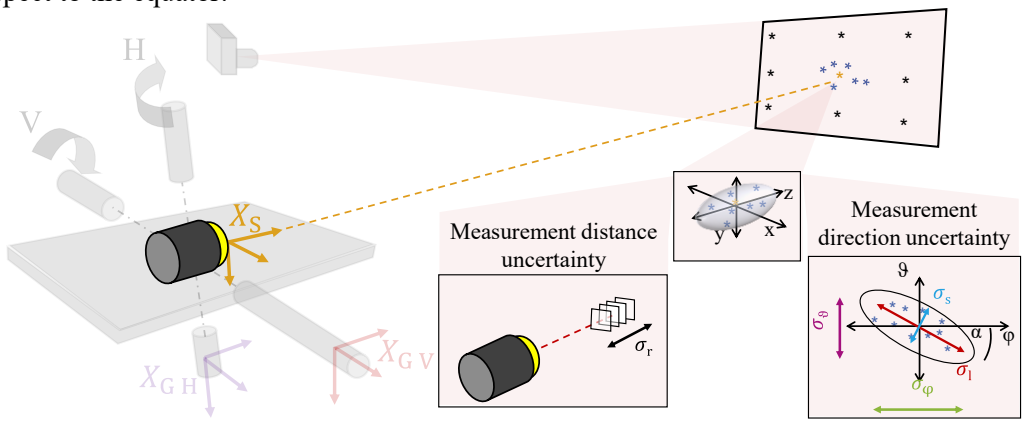


**Figure 8:** Geometric uncertainty evaluation for each measured direction.

## 5. Evaluation results

For a geometric measurement uncertainty analysis Table 2 shows the uncertainty budget. The "maximum absolute contribution of direction" presents the standard uncertainties of the most critical spatial direction from a half-space measurement along the large ellipse axis. The "maximum absolute contribution of distance" presents the same for the measurement distance. To show the influence of all geometric parameters considering correlations, the last two lines give the geometric combined standard uncertainty of the measurement system. Also to make a difference between the measurement system itself and the measurement errors, that occur by taking in account positioning errors of the source and the laser matrix, we differ between an uncertainty of the total system with (no. 24) and without (no. 25) an uncertainty of the DUT and laser matrix positioning. In the second case the uncertainty of no. 1-6 and no. 14-19 is obtained to be zero.

### *5.1. Results concerning goniometer position accuracy solely*

To discuss the result and explain the graphical evaluation method, we will first show the results of a position inaccuracy of the goniometer axis solely during the measurement process (no. 7 and 10). Therefore we assume an uncertainty of the goniometer H- and V-axis positioning with $u(H) = 0.0031°$

and $u(V) = 0.0041°$. Figure 9 shows the confidence regions of nine spatial directions located in 80° intervals, where the middle figure corresponds to the spatial direction (0°,0°). The crosses in Figure 10 also give the spatial directions of the evaluated confidence regions. Moreover, Figure 10 represents the standard uncertainty of the measured direction in the form of the large ellipse axis for each simulated direction. Figure 11 shows the standard uncertainty along the short ellipse axis. The scaling of this and the following diagrams was set to a logarithmic scale describing the uncertainty of the spatial direction from $10^{-3}$° to 1°. The lower end of the scale was set to $10^{-3}$° so that uncertainties up to a decade below the goniometer's specified resolution of 0.01° can be shown. The upper end of the scale was set to 1° to be able to show the maximum uncertainty contribution from the uncertainty budget.

In all three diagrams, the direct transfer of the uncertainty of the goniometer axes to the uncertainty of the measurement direction at the equator can be seen. Meanwhile for measurement directions at the pole just the goniometer V-axis affects the uncertainty. Nevertheless, closer to the pole correlations might be possible.

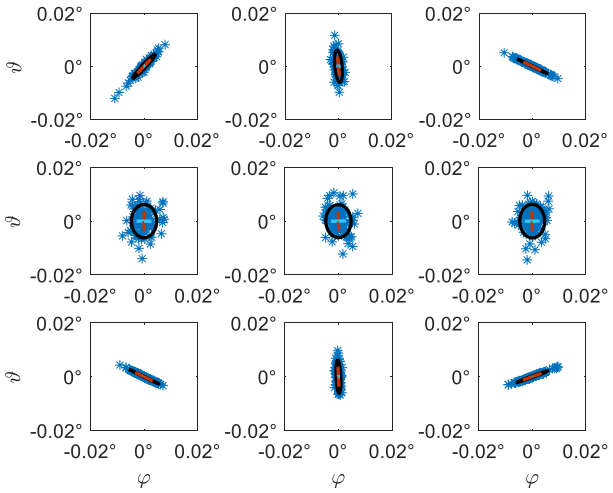


**Figure 9:** Uncertainty of the measurement direction assuming a position inaccuracy of the goniometer-axes solely. The results are given as elliptical confidence regions by the Monte-Carlo-Simulation for nine directions, arranged in 80° intervals ($\varphi \in [-80°, 0°, 80°]$, $\vartheta \in [-80°, 0°, 80°]$).

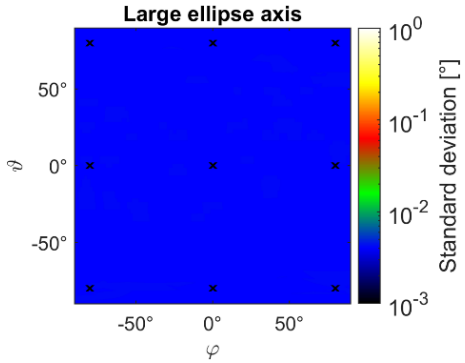


**Figure 10:** Uncertainty of the measurement direction assuming a position inaccuracy of the goniometer-axes solely, given as the standard deviation along the large ellipse axis.

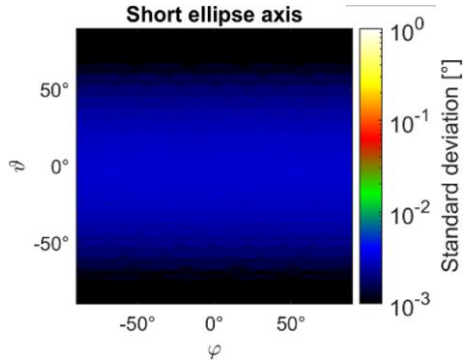


**Figure 11:** Uncertainty of the measurement direction assuming a position inaccuracy of the goniometer-axes solely, given as the standard deviation along the short ellipse axis.

### *5.2. Results concerning the total measurement system*

The direction uncertainty of the whole measurement system is shown in Figure 12 to Figure 14. These figures indicate that the uncertainty of the large ellipse axis equals the uncertainty of the short

ellipse axis over the entire angular region with 0.36°. Thus, there are no relevant correlations by considering the entire measurement system. Figure 15 illustrates the results for the uncertainty of the measurement distance which is also almost constant at 10 mm over the entire measurement region.

In order to identify relevant input quantities, the results from Table 2 and Figure 12 to Figure 14 are examined more in detail. Figure 16 shows the individual contributions to the measurement direction considering the uncertainty along the large ellipse axis. The box plot presents the distribution of the standard uncertainties of all measured directions. The greatest influence is caused by the DUT and laser matrix orientation and corresponds up to 0.25°, which equals the uncertainty of the input parameter. Nevertheless, there are also directions where the influence of the miss orientation is negligible. This depends on the acquisition position of the goniometer. Also the test source position with a contribution of up to 0.057° (see Table 2) affects the measurement. This contribution can be explained by the goniometer screen distance of 10 m as well as the standard positioning uncertainty of 10 mm. The last entry in the list in Figure 16 represents the uncertainties of the total system. This box plot shows the result of Figure 13 in another way. It can be seen, that the uncertainty of each direction is almost the same around 0.36° dominated by the contribution of the DUT and laser. The uncertainty contributions of the measurement distance are shown in Figure 17 without further explanation.

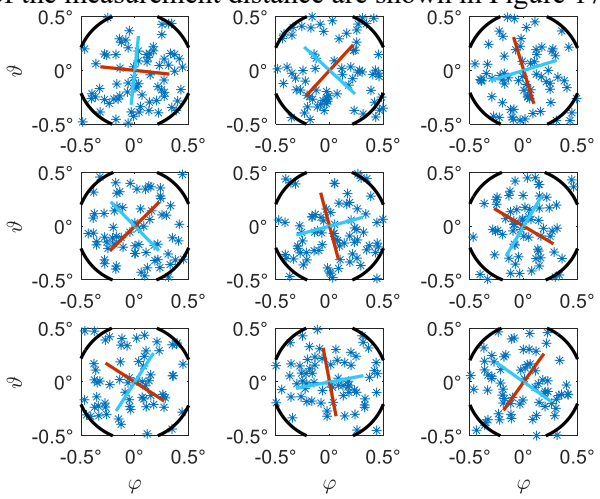


**Figure 12:** Uncertainty of the measurement direction for the total system given as elliptical confidence regions.

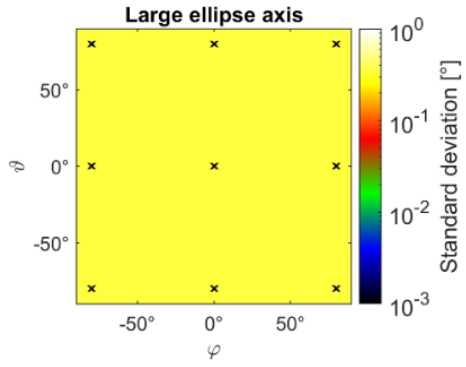


**Figure 13:** Uncertainty of the measurement direction for the total system, given as the standard deviation along the large ellipse axis.

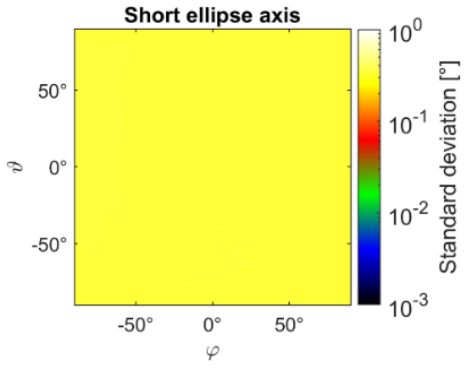


**Figure 14:** Uncertainty of the measurement direction for the total system, given as the standard deviation along the short ellipse axis.

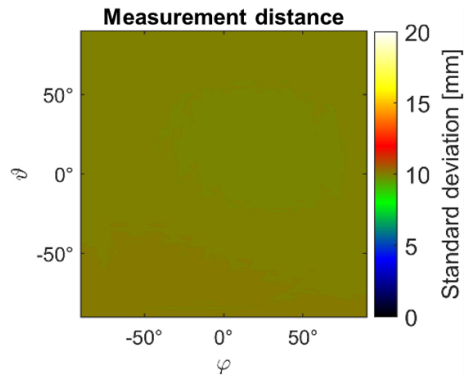


**Figure 15**: Uncertainty of the measurement distance for the total system.

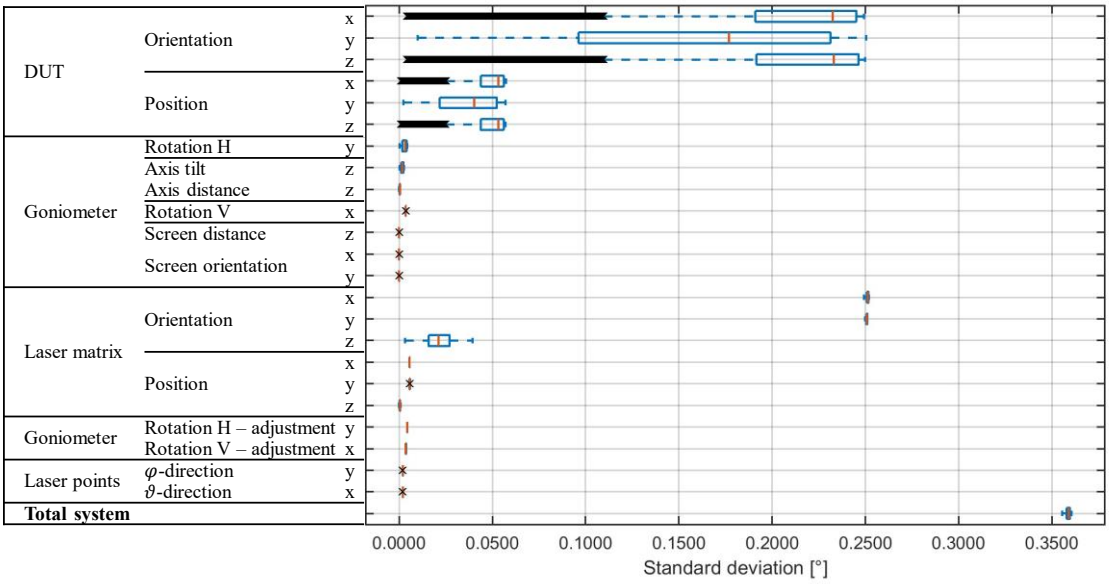


**Figure 16:** Uncertainty of the measurement direction for the total system split up by its individual contributions. The results are given as the standard deviation along the large ellipse axis.

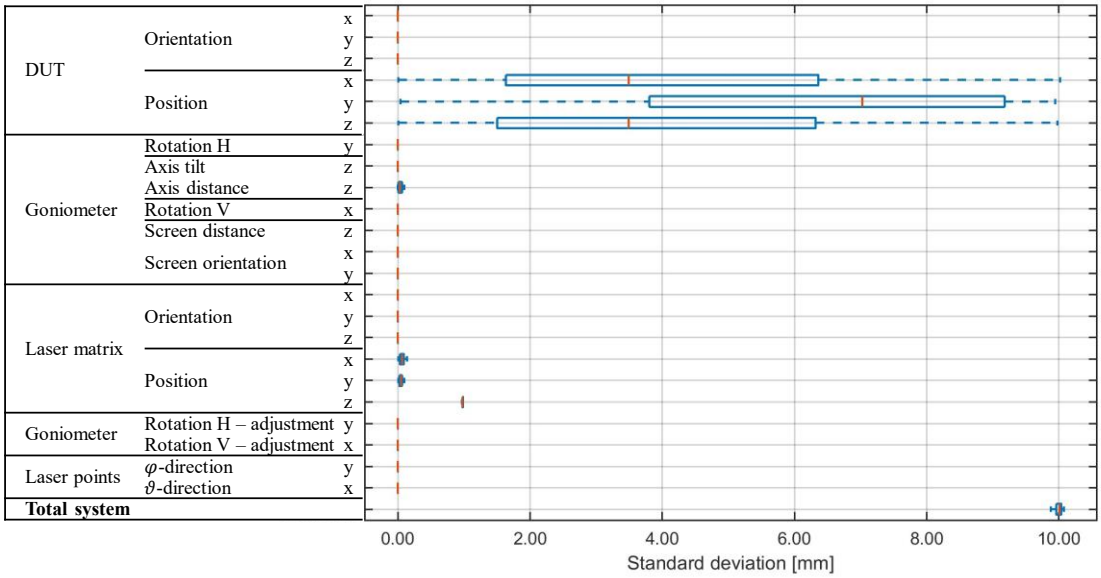


**Figure 17:** Uncertainty of the measurement distance for the total system split up by its individual contributions.

## 6. Conclusion

In this paper we presented a technique based on the MCM according to GUM Supplement 2 to determine the geometric uncertainty parameters “measurement direction” and “measurement distance” of LID measurement systems. A crucial point is the simulation of both the adjustment and measurement process due to the matter that both processes provide uncertainties. Doing so, also correlations of important input quantities are considered. Therefore, we described a process to select necessary input parameter and set up the kinematic chain. With some additional effort this method is transferable to all types of goniophotometer, meanwhile a standardized process to build up the geometric and also

photometric measurement components is necessary. It should also be mentioned that this work solely presents a method to determine the geometric uncertainty of LID measurement systems. So the measurement model might miss some quantities, as for example, the influence of DUT weight on the bending of the goniometer during the measurement.

Finally, the influence of the light source positioning must be discussed. In the simulation of the total system we assumed an uncertainty of the DUT position of 10 mm in each direction. Also we assumed an uncertainty of the DUT and laser matrix orientation with 0.25° around each axis. These input variables provide the largest uncertainty contributions, in part because their standard deviations are larger than those of the other input variables. Now there are individual measurement applications that are not or less sensitive to a DUT misalignment and miss orientation. E.g. the DUT has alignment markings or the LID might be rotated in post processing steps. If required this also may be implemented in the simulation process. To give a first impression how DUT and laser matrix position and orientation changes the results Table 2 shows also the combined uncertainty for the total system without considering source positioning uncertainty. In this case the measurement uncertainty direction reduces to 0.0093°.

## References

[1] Otto Reeb 1962 *Grundlagen der Photometrie (Bücher der Messtechnik Wissenschaftliche Bücherei)* (Karlsruhe: Braun)
[2] Moreno I and Sun C-C 2009 Three-dimensional measurement of light-emitting diode radiation pattern: a rapid estimation *Meas. Sci. Technol.* **20** 75306
[3] Sayanca I L, Trampert K and Neumann C 2018 Indirect light intensity distribution measurement using image merging *Advanced Mathematical and Computational Tools in Metrology and Testing XI (Series on Advances in Mathematics for Applied Sciences)* ed A B Forbes *et al* (WORLD SCIENTIFIC) pp 307–14
[4] Schwanengel C, Reiners T, Schmidt F and Diem C Das Beste aus zwei Welten – Kombination von Goniophotometrie und digitaler Bildverarbeitung *Hrsg. (Hg.) 2016 – LICHT 2016*
[5] Bipm, IEC, IFCC I S, IUPAC, IUPAC I and OIML 2008 JCGM 100:2008 Evaluation of measurement data — Guide to the expression of uncertainty in measurement: GUM 1995 with minor corrections *Joint Committee for Guides in Metrology*
[6] BIPM, IEC, IFCC, ILAC, ISO, IUPAC, IUPAP and OIML 2011 JCGM 102:2011 Evaluation of measurement data – Supplement 2 to the "Guide to the expression of uncertainty in measurement" – Extension to any number of output quantities *Joint Committee for Guides in Metrology*
[7] Jokiel B, Ziegert J C and Bieg L 2001 Uncertainty propagation in calibration of parallel kinematic machines *Precision Engineering* **25** 48–55
[8] Katona M, Trampert K, Neumann C and Schwanengel C 2019 Systemanalyse eines bildgebenden LVK Messsystems mittels Monte Carlo Simulation
[9] Krueger U, Ruggaber B and Blattner P 2020 Measurement Uncertainty in Imaging Photometry: An introduction for TC2-67 based on Excel and Octave *CIE Tutorial on Measurement Uncertainties for Headlamp*
[10] CIE 2011 CIE 198:2011 Determination of Measurement Uncertainties in Photometry (International Commission on Illumination (CIE))
[11] Bronštejn I N and Semendjaev K A 2006 *Taschenbuch der Mathematik* 6th edn (Frankfurt am Main: Deutsch)
[12] Synopsis 2016 *LightTools Enewsletter* https://www.synopsys.com/optical-solutions/e-news/lighttools/osg_lt-december2016.html
[13] Corke P 2017 *Robotics, Vision and Control* vol 118 (Cham: Springer International Publishing)

**Acknowlegement**
This work was financed by the project 19NRM02 RevStdLED which has received funding from the EMPIR programme co-financed by the Participating States and from the European Union's Horizon 2020 research and innovation programme.